RESEARCH ARTICLE

Use of a spatial light modulator as an adaptable phase mask for wavefront coding

G Carles[a], G Muyo[b], S Bosch[a] and A R Harvey[b]

[a]Departament de Física Aplicada i Òptica, Universitat de Barcelona, Martí i Franquès 1, E-08028 Barcelona, Spain.; [b]School of Engineering and Physical Sciences, Heriot-Watt University, Edinburgh, EH14 4AS, UK.

A wavefront-coded imaging system employing a spatial light modulator (SLM) for the agile implementation of phase masks is presented. The SLM is a liquid crystal display that can be modulated to implement cubic phase masks of variable coding strength. These phase masks produce broad point spread functions insensitive to defocus aberration and are used in combination with post-detection digital image processing to extend the depth-of-field of an imaging system. A detailed description of the calibration process of the SLM in phase mode is presented together with experimental results which include wavefront-coded modulation transfer functions and increased depth-of-field images. The most interesting feature is the versatility provided by the imaging system, as compared to conventional (fixed phase mask) designs, and the agility in which it is done.

Keywords: Wavefront Coding, phase mask, spatial light modulator, imaging systems, image processing

1. Introduction

The past decade has witnessed a growth of interest in the use of hybrid optical/digital techniques to provide improved imaging capabilities or extra degrees of freedom in the design of imaging systems (*1*). One such technique, known as wavefront coding (*2–4*) involves placing a refractive coding phase mask in the aperture stop of an imaging system. The mask, typically described by a polynomial function with radial antisymmetry (*5*), modifies and broadens the point-spread-function such that the image is recorded with an aberration-invariant encoding blur. A high quality image is recovered by digital, post-detection inversion of the optical coding such that the complete process of optical coding and digital decoding provides reduced sensitivity to variations in optical aberrations.

The purposes and advantages of this hybrid optical/digital imaging systems are many and diverse (*6–10*): its ability to increase depth-of-focus can be useful not only for increasing depth-of-field in the object domain, but can also enable athermalization and achromatisation of thermal infrared imaging systems (*11*); by reducing sensitivity to aberrations it can be used to reduce lens complexity (e.g. reducing the number of lens elements); or can enable relaxed manufacturing tolerances (*12*). The *quid pro quo* for this performance gain is noise amplification in the restored images.

The most commonly used modulation function for the encoding mask has the form

$$\theta(x,y) = \alpha\left(x^3 + y^3\right) + \beta\left(x^2y + xy^2\right) \tag{1}$$

where x and y are normalised pupil-plane co-ordinates and α and β are coefficients describing the strength of modulation mask. Increasing the strength of the phase mask improves the

ability to mitigate optical aberrations, but through increased suppression of the modulation-transfer-function (MTF) also increases the noise amplification accompanying image recovery. Optimisation of Equation (1) yields values of $\beta = 0$ and $\beta = -3\alpha$ which enable particularly good insensitivity to aberrations (*13*). The purely cubic mask ($\beta = 0$) was synthesised analytically by Dowski and Cathey (*3*), and subsequently the generalised form ($\beta \sim -3\alpha$) was been proposed heuristically and optimised numerically (*14*). The preference for either the purely cubic or the generalised cubic varies with application and lens parameters (*11, 13*) whilst the optimal strength of the phase mask is normally selected as a trade off between noise amplification and aberration mitigation. For example, in the case of defocus, both amount of noise amplification and the maximum defocus (*5*) that can be mitigated varies with the inverse of the strength of the phase mask and hence the optimal value for the strength of wavefront coding is the minimum value that is compatible with mitigation of optical aberrations.

In previously reported applications of wavefront coding, the phase mask is a fixed optical element that is optimised during the design process according to its purpose and the preferred trade of aberration insensitivity against noise amplification. Since this optimal trade may vary with application and circumstances (for example, light level or required depth-of-field) it is beneficial to employ a programmable phase element that can be optimised in real time. We describe here the use of a Spatial Light Modulator (SLM) as a programmable phase plate to enable real-time optimisation of the strength or form of the wavefront-coding function.

In the next section, we describe the calibration of the SLM to enable optimal encoding of the required phase modulation and subsequently implement a cubic phase-function in a wavefront-coded imaging system. We demonstrate that, as required, the cubic phase-mask produces a PSF which is virtually invariant to defocus aberration and a MTF that exhibits no nulls within the passband. The MTF is however highly suppressed and so noise is amplified during image recovery. In section 3, the agile wavefront-coded imaging system is used to acquire coded images of representative scenes with diverse spatial-frequency content and object depths. Finally, restored images with extended depth-of-field are recovered using Wiener filtering and compared with those acquired with a conventional imaging system.

2.   Calibration of the Spatial Light Modulator for wavefront coding

The Spatial Light Modulator (SLM) used in this work is a twisted-nematic liquid-crystal LC2002 from Holoeye (*15*). The device enables electrically modulated birefringence in transmission mode and is controlled by means of a video signal with a resolution 800x600 pixels and 8 bits of depth. To provide modulation the SLM was placed between two linear polarizers and it is the orientation of these two polarizers relative to a reference 'vertical' axis of the SLM (in our experiments the SLM was oriented with the connectors on the top surface) that determine the modulation characteristics of the SLM. The device applies both phase and amplitude modulation simultaneously and a key objective of the calibration is to deduce the orientations of the polarizers that maximise phase modulation whilst minimising amplitude modulation. These were find by a manual optimisation process.

Previous reports have shown that it is possible to obtain better phase-only modulation (increasing slightly the phase modulation depth and decreasing drastically the coupled amplitude modulation) by using elliptic polarization states(*16, 17*). However, as is illustrated above, the coupled amplitude modulation does not have a major influence in the final performance for the application described here, so that the expected reduction in image quality is negligible whilst the associated complexity of implementing and calibrating a system employing elliptically polarized light is avoided. This is particularly significant if the technique is to be extended to broadband operation for which the degree of ellipticity would introduce additional calibration complexity.

In addition, it is necessary to calibrate the gain, offset and non-linearity of the mapping of pixel brightness levels to optical phase modulation. The method that we have adopted for the

calibration of the SLM is described below.

2.1. *Characterization of the SLM*

Several methods have previously been proposed for determining the optimal orientations of the polarizers; for example, it is common to use a Jones matrix analysis to deduce suitable orientations by inspection and modelling (*18–20*). We report here, optimisation using a simple empirical method in which the SLM was used to modulate the light transmitted through two Young's slits illuminated by an expanded laser beam as shown in Fig. 1. Keeping the modulation at one of slits constant (by the application of a grey-level of zero) the differential phase modulation applied by the SLM at the other slits was determined from the phase modulation of the spatial interferogram recorded at the Charge Coupled Device (CCD) detector (*21*).

The optimal orientation of the polarizers is such that the maximum possible phase modulation is achieved whilst maintaining a minimal variation in fringe contrast across all the possible phase modulations (256 grey-levels). A manual optimisation of optimal polarizer orientations yielded two local optima as summarized in Table 1. The first configuration corresponds to the maximum attainable phase modulation while the second configuration, which was used in subsequent experiments, provides a good compromise between high phase-modulation and low amplitude-modulation.

The calibration of the phase modulation consists of recording the fringe displacement as a function of the grey-level applied to the SLM. Various interferometric calibration techniques have been proposed for this purpose (*22, 23*). We employed the setup shown in Figure 1 using light of wavelength 632.8nm from a helium neon laser.

The combined phase and amplitude modulations of the SLM are shown in Figure 2 in a polar representation. It can be observed from Figure 2 that the pair of angles {10,70} for the polarizers produces a phase modulation of 1.55π accompanied by attenuation that varies by a factor of 5.2, whilst the pair of angles {-20,40} produces a slightly reduced phase modulation of 1.48π accompanied by an amplitude modulation that varies by a factor of only 2. We have selected this latter pair of angles to implement the wavefront-coding phase mask. Although Hong *et al.* (*24*) have also used the same SLM to implement a cubic phase mask, their choice of the configuration angles is different from the present work, resulting in a different response; their aim was to find a value of α of the cubic phase mask that suits a particular contrast reduction criteria. Here, we aim at getting an insight in the use of the modulator that optimizes the imaging system performance. For this reason, we have used 51 points along the grey-level range to realise a more accurate calibration and we have used the same monochromatic light of 632.8nm to (a) calibrate the SLM, (b) acquire the PSFs that will be used for the restoration stage and (c) acquire the working scene images.

2.2. *Implementation*

To implement the SLM as a phase mask in a wavefront coding scheme a grey-scale image is calculated using the above non-linear calibration process such that the phase modulation applied to the wavefront approximates that required for wavefront coding. The maximum phase modulation that may be applied is a little less than 2π whereas the required peak-to-peak modulation will typically be several waves so that the optical phase modulation is applied modulo 2π. In addition to the 2π phase steps, because the maximum phase modulation is about $\pi/2$ less than 2π there will be phase discontinuities of about $\pi/2$ in the transmitted wavefront, which will lead to a phase modulation error of about $\pi/4$ between desired and obtained wavefronts (see Figure 4). Phase mismatches this small will not produce significant reductions in the Strehl ratio of the imaging system.

We have implemented the phase calibration using a look-up table with linear interpolation as depicted in Figure 3. It can be observed from Figure 3 that a linear phase response is obtained

with good fidelity apart from an inability to produce phase modulations between 1.48π and 2π. Since most common phase masks are relatively flat at the centre, a modulation of π radians is fixed here to avoid a sharp step in the modulation and also forcing the symmetry of the profile centred at π radians. Figure 4 shows an example summarizing the process of mapping the grey-levels to obtain a cubic profile modulation.

The calibrated SLM was then used to implement a wavefront-coded imaging system as depicted in Figure 5. An iris diaphragm controls the aperture of the SLM. After transmission through the SLM, light is brought to focus by a Nikon F/4 300mm-focal-length lens onto the sensor of a low-noise CCD. For practical reasons, the SLM cannot be exactly placed in the aperture stop of the optical system —the optimum location for the mask that applies identical coding for all field positions— however the small field-of-view in this demonstration means that this effect has negligible impact.

In the next section, we present a series of results exploring the compromise between extension of the depth-of-field, the strength of the coding and noise amplification, also evaluating the final image quality.

3.   Results

We present here results following image restoration, which for simplicity is a simple Wiener filter. The MTF is computed by Fourier transformation of the acquired PSF, which is slightly under-sampled. The sagittal MTFs with and without cubic phase mask ($\alpha = 2\lambda$) for different magnitudes of defocus aberration are shown in Figure 6. Also shown are the wavefront-coded MTFs after restoration. The defocus errors correspond to distances of 2, 4 and 8 cm far from the in-focus object plane, equivalent to defocus coefficients W_{20} of 1, 2 and 4 wavelengths respectively. All the evaluation experiments are done using monochromatic incoherent light at 632.8 nm, to fit with the calibration results.

The restoration process operates on the coded MTF and attempts to recover the diffraction limited features of the optical system. It can be observed from Figure 6 that most of the restored MTFs are practically indistinguishable from the diffraction limited MTF. This defocus alleviation results in an increased depth-of-field with respect to the conventional imaging system. However, if defocus is high enough, the coding cannot provide sufficient invariance and the coded MTF drops. Another important fact worth noting is that wavefront coding by means of a cubic phase mask produces MTFs with no nulls so the restoration process is not ill-posed. On the contrary, traditional defocused MTFs exhibit zeros which jeopardize the restoration process.

Analogous results are shown in Figure 7 with a coding strength of $\alpha = 5\lambda$. It can be clearly seen how the depth-of-field is further increased, although the highly-oscillatory modulations apparent in the MTFs may result in artefacts in the restored images. Furthermore, in the case of higher amplitude of phase coding, the coded MTFs become highly suppressed and the restoration process gives rise to greater noise amplification. All data in Figure 6 and Figure 7 is experimental.

To visually illustrate the improvement in depth-of-field, various targets are imaged with and without a cubic phase mask ($\alpha = 5\lambda$). The coded images are subsequently restored using a unique deconvolution kernel, the in-focus cubic PSF, and Wiener filtering. The results are shown in Figure 8 and Figure 9. The depth-of-field extension is clearly evident; for example, nulls and phase reversal characteristics of a defocused system (left column) are not present in the restored wavefront-coded images (right column). The centre column of Figure 8 shows the restoration of the non-coded images in the left column using each defocused PSF kernel (note that each image needs a different restoration kernel) for comparison. It can be seen that there is loss of image information at spatial frequencies for which nulls occur in the MTF, resulting in substantially poorer quality images. Moreover, in the case of Figure 9 the same simple restoration procedure for the non-coded images is not possible because the PSF varies substantially with range across the field of view, whereas it is possible with the wavefront-coding method since the PSF is approximately invariant. Finally, this extension of the depth-of-field occurs at the cost of noise

amplification in the restored images.

4.   Conclusions

This work presents a study of the use of an SLM as a phase mask for the wavefront codification to provide flexibility and versatility to hybrid optical/digital imaging systems. The SLM LC2002 from Holoeye is accurately calibrated and the configuration is set to provide the desired phase codification with agility. Several experiments have been performed demonstrating the usability of the SLM as a phase mask. The results show a good imaging performance in terms of signal-to-noise ratio and defocus aberration mitigation.

The flexibility and ease-of-use supplied with the use of a SLM for the coding allows devising adaptable procedures, mainly as compared with the use of fixed (manufactured) glass phase masks. This flexibility allows the imaging system be optimised for a wide range of applications. Finally, the analysis presented here can be of assistance during the design and manufacturing process of future phase elements since the SLM provides a means of implementing numerous types of phase masks at a low cost.

Acknowledgements

References

(1) Mait, J.; Athale, R.; van der Gracht, J. Evolutionary paths in imaging and recent trends. *Opt. Express* **2003**, *11* (18) (SEP 8), 2093–2101.
(2) Cathey, W.T.; Frieden, B.R.; Rhodes, W.T.; et al. Image gathering and processing for enhanced resolution. *J. Opt. Soc. Am. A* **1984**, *1* (3), 241–250.
(3) Edward R. Dowski, J.; Cathey, W.T. Extended depth of field through wave-front coding. *Appl. Optics* **1995**, *34* (11), 1859–1866.
(4) Bradburn, S.; Cathey, W.; Dowski, E. Realizations of focus invariance in optical-digital systems with wave-front coding. *Appl. Optics* **1997**, *36* (35) (DEC 10), 9157–9166.
(5) Muyo, G.; Harvey, A. Decomposition of the optical transfer function: wavefront coding imaging systems. *Opt. Lett.* **2005**, *30* (20) (OCT 15), 2715–2717.
(6) Cathey, W.; Dowski, E. New paradigm for imaging systems. *Appl. Optics* **2002**, *41* (29) (OCT 10), 6080–6092.
(7) Kubala, K.; Dowski, E.; Cathey, W. Reducing complexity in computational imaging systems. *Opt. Express* **2003**, *11* (18), 2102–2108.
(8) vanderGracht, J.; Dowski, E.; Taylor, M.; et al. Broadband behavior of an optical-digital focus-invariant system. *Opt. Lett.* **1996**, *21* (13) (JUL 1), 919–921.
(9) Mezouari, S.; Harvey, A. Phase pupil functions for reduction of defocus and spherical aberrations. *Opt. Lett.* **2003**, *28* (10) (MAY 15), 771–773.
(10) Mezouari, S.; Muyo, G.; Harvey, A. Circularly symmetric phase filters for control of primary third-order aberrations: coma and astigmatism. *J. Opt. Soc. Am. A* **2006**, *23* (5) (MAY), 1058–1062.
(11) Muyo, G.; Singh, A.; Andersson, M.; Huckridge, D.; Wood, A.; et al. Infrared imaging with a wavefront-coded singlet lens. *Opt. Express* **2009**, *17* (23) (NOV 9), 21118–21123.
(12) Demenikov, M.; Findlay, E.; Harvey, A.R. Miniaturization of zoom lenses with a single moving element. *Opt. Express* **2009**, *17* (8), 6118–6127.
(13) Vettenburg, T.; Wood, A.; Bustin, N.; et al. Optimality of pupil-phase profiles for increasing the defocus tolerance of hybrid digital-optical imaging systems. In: *Proc. SPIE - The International Society for Optical Engineering*, Vol. 7429; p. 742903 (8 pp.).
(14) Prasad, S.; Torgersen, T.; Pauca, V.; Plemmons, R.; et al. High-resolution imaging using integrated optical systems. *Int. J. Imag. Syst. Tech.* **2004**, *14* (2), 67–74.
(15) Spatial Light Modulator LC2002. HOLOEYE Photonics AG. www.holoeye.com. .
(16) Marquez, A.; Iemmi, C.; Moreno, I.; Davis, J.; Campos, J.; et al. Quantitative prediction of the modulation behavior of twisted nematic liquid crystal displays based on a simple physical model. *Opt. Eng.* **2001**, *40* (11), 2558–2564.
(17) Nicolas, J.; Campos, J.; Yzuel, M. Phase and amplitude modulation of elliptic polarization states by nonabsorbing anisotropic elements: application to liquid-crystal devices. *J. Opt. Soc. Am. A* **2002**, *19* (5), 1013–1020.
(18) Yamauchi, M.; Eiju, T. Optimization of twisted nematic liquid-crystal panels for spatial light phase modulation. *Opt. Commun.* **1995**, *115* (1-2) (MAR 1), 19–25.

6   *REFERENCES*

(19) Durán, V.; Lancis, J.; Tajahuerce, E.; et al. Poincaré Sphere Method for Optimizing the Phase Modulation Response of a Twisted Nematic Liquid Crystal Display. *J. Disp. Tech.* **2007**, *3* (1), 9–14.

(20) Moreno, I.; Velasquez, P.; Fernandez-Pousa, C.R.; Sanchez-Lopez, M.M.; et al. Jones matrix method for predicting and optimizing the optical modulation properties of a liquid-crystal display. *J. Appl. Phys.* **2003**, *94* (6), 3697–3702.

(21) Retiga 1300. QIMAGING. www.qimaging.com. .

(22) Hongxin Zhang; Jian Zhang; Liying Wu Evaluation of phase-only liquid crystal spatial light modulator for phase modulation performance using a Twyman-Green interferometer. *Meas. Sci. Technol.* **2007**, *18* (6) (June), 1724–8.

(23) Engström, D.; Milewski, G.; Bengtsson, J.; et al. Diffraction-based determination of the phase modulation for general spatial light modulators. *Appl. Optics* **2006**, *45* (28), 7195–7204.

(24) Hong, D.; Park, K.; Cho, H.; et al. Flexible depth-of-field imaging system using a spatial light modulator. *Appl. Optics* **2007**, *46* (36) (DEC 20), 8591–8599.

Table 1.   Results for two different configurations. P: angle of the polarizer, A: angle of the analyzer, C: contrast of the LCD, B: brightness of the LCD, T_{min}: minimum intensity transmittance along the grey-level range, δ_{max}: maximum phase modulation. The configuration controls relative to the gamma correction are set to 0.

	P	A	C	B	T_{min}	δ_{max}
Configuration 1:	10°	70°	200	100	2.8%	1.56π
Configuration 2:	-20°	40°	200	100	22.1%	1.48π
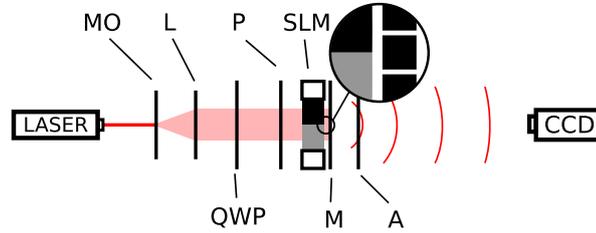
Figure 1.   Set of a double hole Young's experiment. MO: Microscope objective, L: lens, QWP: Quarter wave plate, P: polarizer, SLM: Spatial Light Modulator, M: mask with two holes, A: Analyzer.
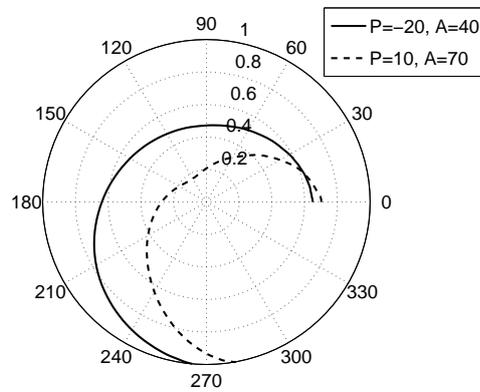
Figure 2.   Modulation behaviour of the SLM with two different configurations. The representation is in polar coordinates (phase and amplitude modulation) and the lines go from the black (0°) to the white (maximum phase attained) along the grey scale. The amplitude is normalized.
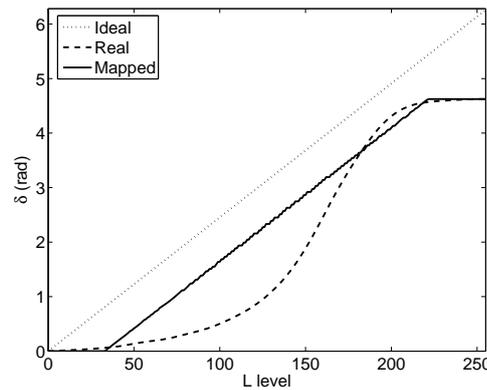

Figure 3.   Phase modulation versus grey-level. The dotted line is the ideal response, the dashed line is the real response (obtained in the calibration process) and the continuous line is the result of applying the look-up-table (the operational response).
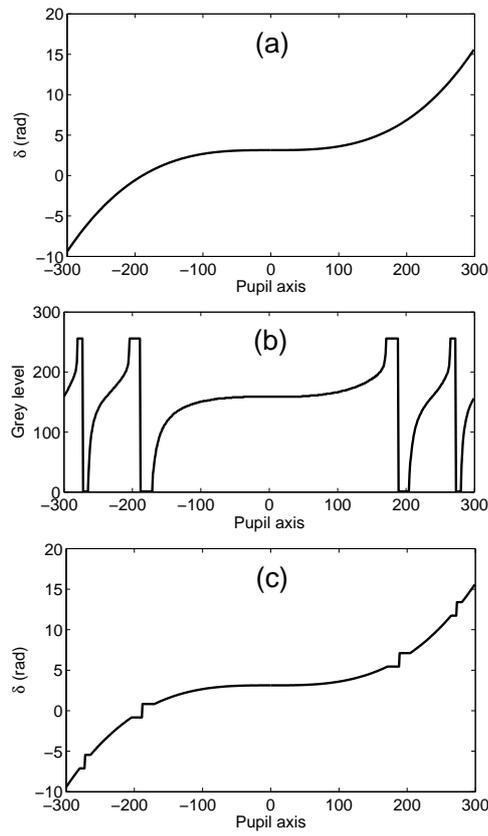
Figure 4. (a) Ideal modulation in a one-dimensional cubic phase mask, (b) grey-level after 2π-folding and mapping the phase (needed to obtain the desired modulation) and (c) actual obtained phase modulation. The horizontal axis represents the discretization in the pupil plane.
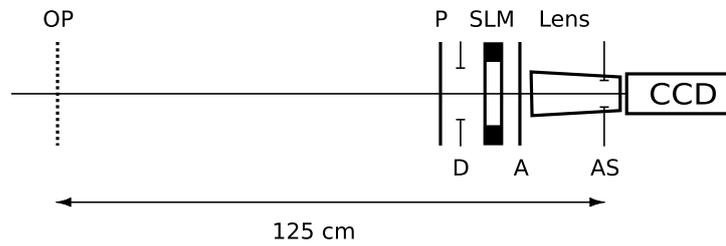

Figure 5. Optical system. OP: object plane situated 125 cm from the camera, P: polarizer, D: iris diaphragm, SLM: Spatial Light Modulator, Lens: 300mm focal length lens, AS: aperture stop, CCD: CCD-camera.
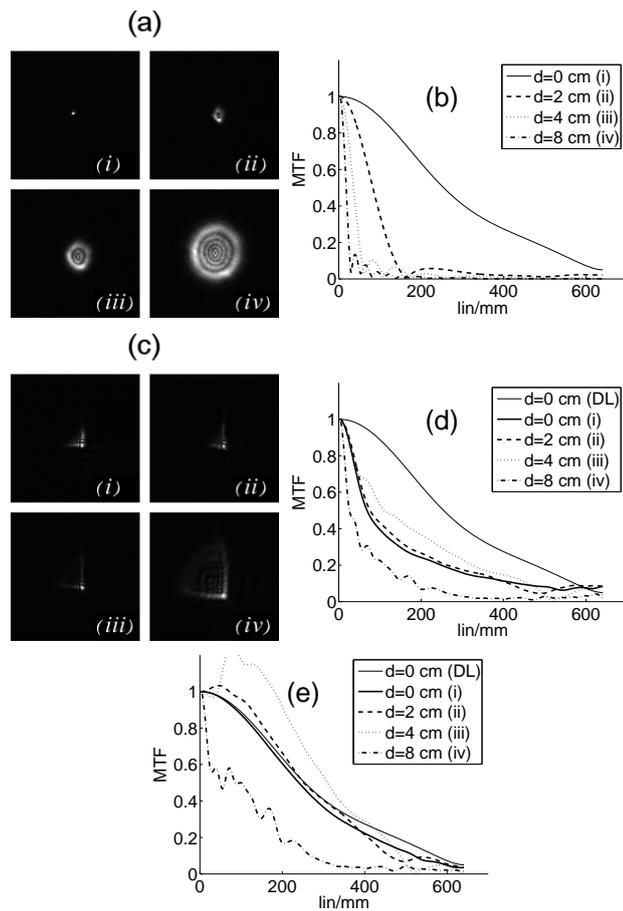
Figure 6.   PSF and MTF of the optical system in the in-focus plane and with three different defocus distances. Images (a) and (c) are the PSF of the traditional and wavefront coded system (using a cubic phase mask with $\alpha = 2$), respectively, in (*i*) the infocus plane and (*ii*) 2 cm, (*iii*) 4 cm and (*iv*) 8 cm far. The graphs show (b) the MTF of the traditional non-coded system, (d) the MTF of the coded system and (e) the restored MTF of the coded system (using the parametric Wiener filter with $k = 0.003$). In graphs (d) and (e) there is also the in-focus diffraction limited MTF (fine lines) for comparison.
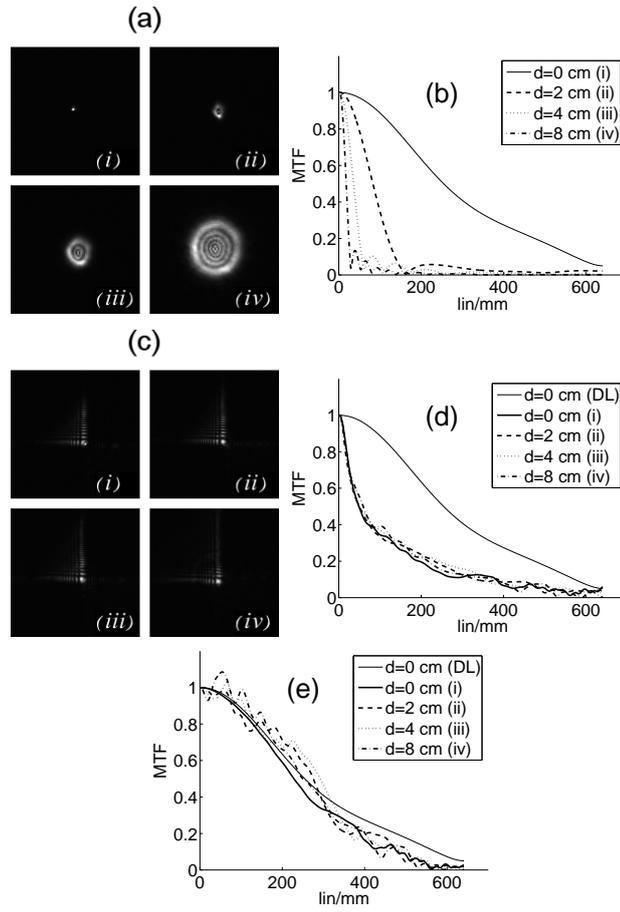
Figure 7.   PSF and MTF of the optical system in the in-focus plane and with three different defocus distances. Images (a) and (c) are the PSF of the traditional and wavefront coded system (using a cubic phase mask with $\alpha = 5$), respectively, in (i) the infocus plane and (ii) 2 cm, (iii) 4 cm and (iv) 8 cm far. The graphs show (b) the MTF of the traditional non-coded system, (d) the MTF of the coded system and (e) the restored MTF of the coded system (using the parametric Wiener filter with $k = 0.003$). In graphs (d) and (e) there is also the in-focus diffraction limited MTF (fine lines) for comparison.
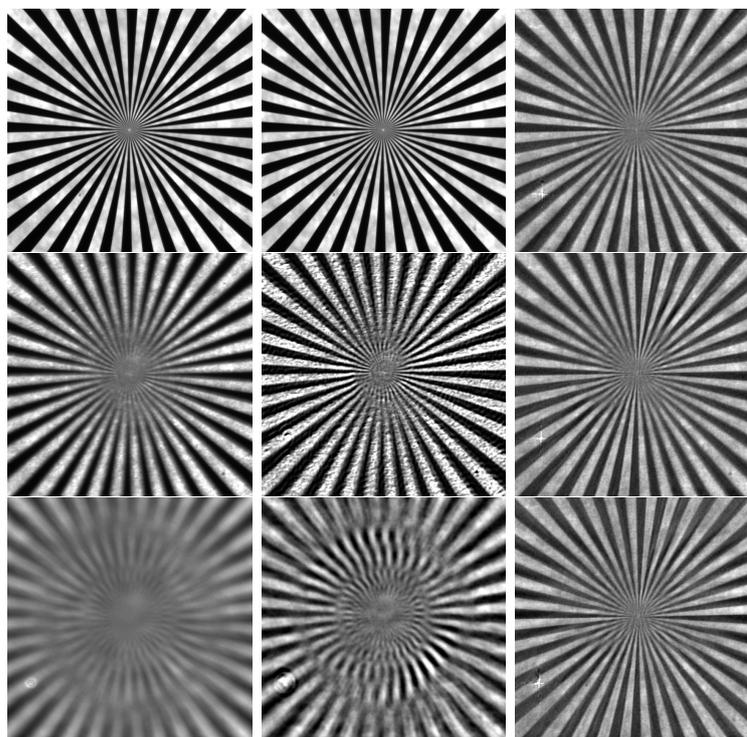
Figure 8. Spoke wheel target situated at defocus distances of 0, 2, and 5 cm. Images in the left column are non-coded. Images in the center column are non-coded and restored using the parametric Wiener filter with $k = 0.005$ and their corresponding PSF (note that the restoration filter is different for each). Images in the right column are coded using cubic phase mask of $\alpha = 5$ and restored using the parametric Wiener filter with $k = 0.005$ (note that the restoration is done using the same filter for each).

Figure 9. Images of deep scenes. Left images are non-coded and right images are obtained with codification (using cubic phase mask of $\alpha = 5$) and restoration (using the parametric Wiener filter with $k = 0.005$).